Journal of Alloys and Compounds 817 (2020) 152716

Contents lists available at ScienceDirect

Journal of Alloys and Compounds

journal homepage: http://www.elsevier.com/locate/jalcom

Origin of photoluminescence from antimony selenide

M. Grossberg [a, *], O. Volobujeva [a], A. Penežko [a], R. Kaupmees [a], T. Raadik [a], J. Krustok [a, b]

[a] Department of Materials and Environmental Technology, Tallinn University of Technology, Ehitajate Tee 5, 19086, Tallinn, Estonia
[b] Division of Physics, Tallinn University of Technology, Ehitajate Tee 5, 19086, Tallinn, Estonia

ARTICLE INFO

Article history:
Received 26 July 2019
Received in revised form
15 October 2019
Accepted 16 October 2019
Available online 17 October 2019

Keywords:
Sb_2Se_3
Photoluminescence
Defects
Donor-acceptor pairs

ABSTRACT

Antimony selenide (Sb_2Se_3) absorber material has great potential for low-cost photovoltaics due to its excellent optoelectronic properties and low processing temperatures. This study presents detailed temperature and excitation power dependent photoluminescence (PL) analysis of Sb_2Se_3 polycrystals revealing the dominating radiative recombination mechanisms and related defects in the studied material. The low-temperature (T = 10 K) PL spectrum consisted of three bands at 0.94 eV, 1.10 eV and 1.24 eV, the last one located close to the low-temperature band gap of Sb_2Se_3 1.32 eV. The PL bands at 1.24 eV and 0.94 eV were found to originate from the donor-acceptor pair recombination, the first one at 1.24 eV involving more distant pairs while the second one at 0.94 eV resulting from the deep acceptor – deep donor pair recombination. Third PL band at 1.10 eV is proposed to be related to the grain boundaries.

1. Introduction

Antimony selenide (Sb_2Se_3) belongs to V_2–VI_3 (V = As, Sb, Bi; VI = S, Se, Te) binary materials that have been attracting research interest due to their potential applications in photovoltaic and thermoelectric devices, as well as in Li- and Na-ion batteries [1–3]. Its constituent elements are of low-toxicity, earth-abundant, and inexpensive. Sb_2Se_3 is a p-type material with high absorption coefficient ($>10^5\ cm^{-1}$ at short wavelength [4]) and nearly optimal band gap energy for solar energy conversion around 1.2 eV at T = 300 K [5]. Solar cells based on core-shell structured Sb_2Se_3 nanorod array have recently reached efficiencies of 9.2% [6].

From the structural properties point of view, Sb_2Se_3 is a one-dimensional line type compound consisting of covalently bonded $(Sb_4Se_6)_n$ ribbons that are stacked together by van der Waals forces and crystallizing in orthorhombic crystal structure with space group *Pbnm* [6]. The Sb_2Se_3 grains can grow in a columnar manner enabling effective charge carrier transport in one direction. Both, direct and indirect band gap of Sb_2Se_3 have been detected [6,7]. Chen et al. [7] determined indirect band gap $E_{g,\ i} = 1.03 \pm 0.01$ eV and direct band gap of $E_{g,\ d} = 1.17 \pm 0.02$ eV at 300 K from the optical absorption measurements of Sb_2Se_3 thin films. The energetic difference between the indirect and direct band gap of Sb_2Se_3 decreases towards lower temperatures and was found to be only 0.04 eV at T = 0 K.

Defects in the absorber material play a crucial role in determining the solar cell performance. There is very little information available about the defects in Sb_2Se_3. Recently, a comprehensive study of the first-principles calculations of the defects in Sb_2Se_3 was published by Huang et al. [8] stating that due to the low symmetry of the quasi-one-dimensional structure of Sb_2Se_3, a series of donor and acceptor levels are predicted in the band gap of the material since each point defect located at non-equivalent atomic sites can have very different properties. Even the presence of some uncommon defects in binary chalcogenide compounds such as the two-anion-replace-one-cation antisite $2Se_{Sb}$ producing a shallow acceptor level is predicted by the theoretical calculations in the same study [8].

The ab initio calculations predict V_{Sb} and Se_{Sb} as dominant acceptor defects in Se-rich Sb_2Se_3 that is aimed for the PV applications [8–10]. Chen et al. [11] and Liu et al. [10] have experimentally determined an acceptor defect level with $E_a = 111$ meV and $E_a = 107$ meV from the temperature dependent conductivity measurements, respectively. It was assigned to Se_{Sb} defect as it is predicted by theoretical calculations as the defect with the lowest formation energy in Sb_2Se_3 with the energy level at about 0.1 eV above the valence band edge [8,10]. The same defect was detected also in admittance spectroscopy measurements with $E_a = 95$ meV and the density of defects states about

* Corresponding author.
E-mail address: maarja.grossberg@taltech.ee (M. Grossberg).

https://doi.org/10.1016/j.jallcom.2019.152716
0925-8388/

1×10^{15} $cm^{-3}eV^{-1}$ [11]. The two deep acceptor defects with energy levels at E_V+0.48 eV and E_V+0.71 eV detected in Sb_2Se_3 by deep level transient spectroscopy (DLTS) were assigned to V_{Sb} and Se_{Sb}, correspondingly [12]. The donor defect at $E_C - 0.61$ eV detected in the same DLTS study, was assigned to Sb_{Se} donor. Recently, Tao et al. [13] published a temperature dependent admittance spectroscopy study on Sb_2Se_3 solar cells with an efficiency of over 7% and detected the presence of three deep defect levels at 363 meV, 398 meV, and 435 meV, however, no assignment of the defects is provided to the reader. Interestingly, it was also found in Ref. [12] that in different samples, the defect densities of Se_{Sb} and Sb_{Se} are always very similar suggesting that they might form [Se_{Sb} + Sb_{Se}] defect complexes as is also predicted in the recent study by Huang et al. [8].

Photoluminescence is a valuable tool for studying recombination mechanisms and related defects in a semiconductors, however, no defect studies of Sb_2Se_3 by luminescence methods could be found in the literature. Only a low-temperature (T = 7 K) PL spectra of Sb_2Se_3 thin films were reported by Shongalova et al. [14], where the presence of two broad (~100 meV) deep PL bands at 0.75 eV and 0.85 eV is detected. However, there is no analysis of the data presented to the reader. Hence, the aim of this study is to fulfil the gap and provide a detailed analysis of the PL spectra of high quality Sb_2Se_3 polycrystals to reveal the radiative recombination mechanisms and related defects.

2. Experimental

The 5 N purity Sb_2Se_3 polycrystals from Alfa Aesar were post-annealed in isothermal sealed quartz ampoules at T = 623 K in Ar atmosphere (100 Torr) in the presence of additional Se source for 30 min as these were found to be the optimal post-treatment conditions for Sb_2Se_3 thin films studied in parallel in order to obtain photoconductive Sb_2Se_3 with uniform stoichiometric composition.

The elemental and phase composition of the sample were determined by Energy Dispersive X-ray spectroscopy (EDX) and Raman spectroscopy. The EDX analysis was performed on Zeiss Merlin high-resolution scanning electron microscope equipped with the Bruker EDX-XFlash6/30 detector. According to the EDX analysis, the Sb_2Se_3 samples have close to stoichiometric composition, being very slightly Se-rich. Micro-Raman spectra were recorded by using a Horiba's LabRam HR800 spectrometer with a 532 nm laser line with the spot size of 10 μm in diameter. The crystal structure of the studied Sb_2Se_3 was determined by X-ray diffraction (XRD) by using a Rigaku Ultima IV diffractometer with monochromatic Cu Kα1 radiation (λ = 1.5406 Å) at 40 kV and 40 mA operating with the silicon strip detector D/teX Ultra. The lattice constants were determined using the Rietveld refinement procedure by Rigaku PDXL version 1.4.0.3 software.

A 0.64 m focal length single grating (600 mm^{-1}) monochromator and the 442 nm line of a He–Cd laser with different power and spot size of 100 μm in diameter were used for the PL measurements. For PL signal detection a Hamamatsu InGaAs photomultiplier tube was used. A closed-cycle helium cryostat was employed to measure temperature dependencies of the PL spectra at temperatures from 10 K to 300 K.

The photoreflectance (PR) measurements were made with a traditional setup [15] where the f = 64 cm grating monochromator together with a 250 W halogen bulb was used as a primary beam and a 45 mW He–Cd laser (441 nm) as a secondary beam. The reflectance signal at 85 Hz was detected using a Si detector with a lock-in amplifier in the spectral range from 1.1 to 1.3 eV.

3. Results and discussion

3.1. Structural properties

The XRD pattern and the Raman spectrum of the studied Sb_2Se_3 polycrystals are presented in Fig. 1a and Fig. 1b, respectively. According to the XRD analysis, the material crystallizes in orthorhombic structure of Sb_2Se_3 with space group *Pnma 62* (ICDD: 01-083-7430). All detected XRD peaks belong to Sb_2Se_3, only main diffraction peaks are labelled for the clarity of the figure. The following lattice parameters were determined: a = 1.17833(10) nm, b = 0.39776(6) nm and c = 1.1634(2) nm being in correspondence with the data reported by other research groups [16].

The characteristic Raman spectrum of the studied Sb_2Se_3 consisted of 6 Raman peaks at 99, 125, 155, 185, 191 and 213 cm^{-1}, the Raman peak at 191 cm^{-1} being the dominant one. The obtained Raman spectrum is in good correlation with the recently published data by Shongalova et al. [17] showing that the often found Raman mode around 250 cm^{-1} that is absent in our samples is corresponding to Sb_2O_3 instead of Sb_2Se_3. No contribution from the secondary phases to the XRD pattern and to the Raman spectrum of the studied material could be detected.

3.2. Photoreflectance and photoluminescence results

For determining the band gap of the studied Sb_2Se_3 polycrystals,

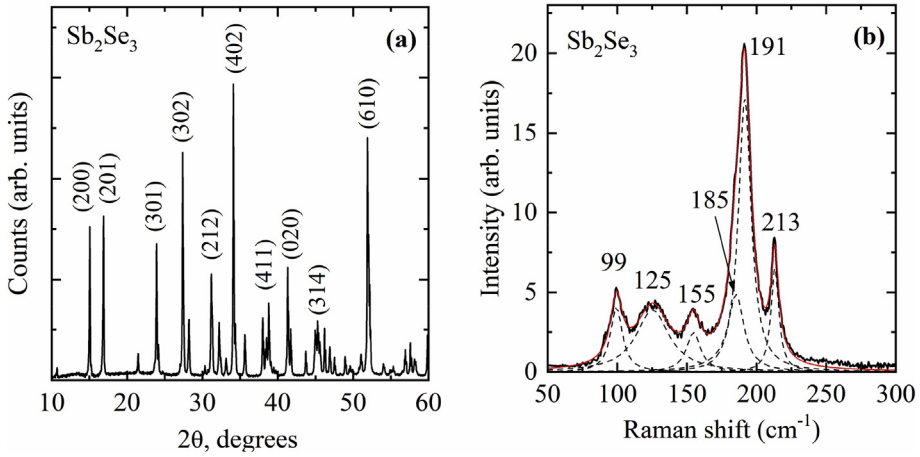

Fig. 1. The XRD pattern (a) and the Raman spectrum (b) of the studied Sb_2Se_3 polycrystals indicating to the single phase material.

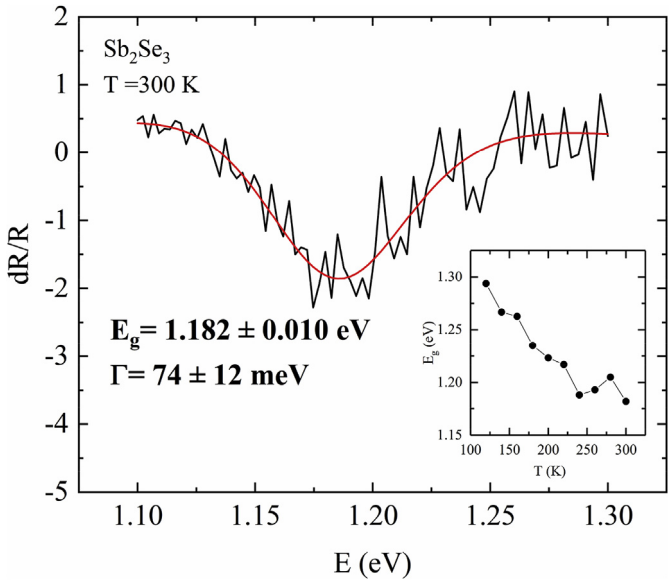

Fig. 2. PR spectrum of the studied Sb_2Se_3 crystals at T = 300 K. The red solid line presents the fitting of the experimental data with Eq. (1). The inset graph presents the temperature dependence of the bandgap energy of the material determined from the PR spectra in the temperature region from 120 K to 300 K. (For interpretation of the references to colour in this figure legend, the reader is referred to the Web version of this article.)

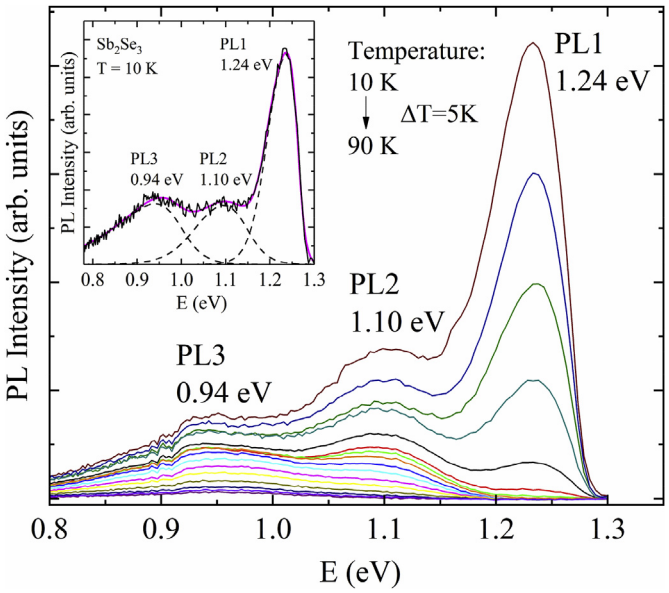

Fig. 3. The temperature dependence of the PL spectrum of the studied Sb_2Se_3 polycrystals. The inset figure presents an example of the fitting of the spectra.

photoreflectance spectroscopy in the temperature range from 120 K to 300 K was used. The PR spectrum of Sb_2Se_3 at T = 300 K is presented in Fig. 2. The measured PR spectra were analyzed by the low-field line-shape function with a third derivative functional form, developed by Aspnes [18]:

$$\frac{\Delta R}{R} = Re\left[Ae^{i\phi}(E - E_g + i\Gamma)^{-n}\right], \quad (1)$$

where E is the photon energy and A, ϕ, E_g, and Γ are the amplitude, phase, optical transition energy, and broadening parameter of the spectrum, respectively. The exponent n in Eq. (1) depends on the type of the critical point, and determining its proper value is of particular importance in analyzing PR spectra. $n = 2.5$, corresponding to a three-dimensional critical point, was used for the fitting of all PR spectra. The band gap $E_g = 1.182 \pm 0.010$ eV and the broadening parameter $\Gamma = 74 \pm 12$ meV were found for Sb_2Se_3 at T = 300 K. The temperature dependence of the bandgap energy of Sb_2Se_3 presented in the inset graph of Fig. 2 is in very good agreement with the data presented in Ref. [5], however, they found slightly larger broadening parameter $\Gamma = 82$ meV at T = 300 K.

The temperature dependence of the PL spectrum of the studied Sb_2Se_3 polycrystals in the temperature region from T = 10 K to T = 90 K is presented in Fig. 3. The inset graph presents the fitting of the spectrum at T = 10 K with an empirical asymmetric double sigmoid function [19] resulting in three PL bands positioned at 1.24 eV (PL1), 1.10 eV (PL2) and 0.94 eV (PL3). The PL bands have slightly asymmetric shape with a steeper decline at high-energy side and a nearly temperature independent incline at the low-energy side that is common in semiconductors with band tails [20]. The average depth of the band edge fluctuations determined from the low energy side of the PL1 band at T = 10 K according to Ref. [20] is $\gamma = 17$ meV, which is smaller than the Urbach energy 38 meV at T = 300 K found by Chen et al. in Ref. [11] indicating to the good quality of our studied polycrystals.

The temperature dependence of the PL bands positions (Fig. 4a) revealed a slight shift towards higher energies in the case of the PL1 and PL3 bands. PL2 band peak position shows a red-shift larger than the temperature dependence of the band gap [5]. The thermal activation energies for the bands obtained from the Arrhenius plot (Fig. 4b) where the dependence of lnI(T) versus 1000/T at high temperatures was fitted by using theoretical expression for discrete energy levels [21]:

$$\Phi(T) = \frac{\Phi_0}{1 + \alpha_1 T^{3/2} + \alpha_2 T^{3/2} \exp(-E_T/kT)}, \quad (2)$$

where Φ is integrated intensity, α_1 and α_2 are the process rate parameters and E_T is the thermal activation energy. As predicted by the fast quenching of the PL spectra with temperature (see Fig. 3) small thermal activation energies $E_{T(PL1)} = 33 \pm 5$ meV, $E_{T(PL2)} = 65 \pm 6$ meV and $E_{T(PL3)} = 93 \pm 3$ meV were obtained.

Considering the low temperature band gap of Sb_2Se_3 $E_g = 1.32$ eV [5,7], the positions of the detected PL bands at T = 10 K being quite distant from the band gap, and the obtained small thermal activation energies, one can propose that the PL1 and PL3 bands most probably arise from the donor-acceptor pair (DAP) recombination. The presence of high concentration of donor-acceptor pairs is also predicted by the theoretical calculations [8].

To analyze the recombination mechanisms behind the PL bands, also the laser power dependence of the PL spectra was measured at T = 10 K, see Fig. 5. The inset graphs present the laser power dependencies of the PL bands positions and intensities. The dependence of the integrated intensity Φ (P) of PL bands on the excitation laser power P is following the dependence $\Phi \sim P^m$ as can be seen from the inset graph in Fig. 5. The power coefficient m can be found as the gradient of the $\Phi(P)$ plot on a log-log scale as shown in upper inset graph in Fig. 5 giving m ~0.6 for all three PL bands. The detected m value which is smaller than unity indicates to the radiative recombination of charge carriers localized at defects within the band gap for all three PL bands [22].

The peak position of the PL2 and PL3 bands varied only slightly (less than 1 meV/decade) with the laser power. A blueshift of the PL1 band with increasing excitation power was detected with the magnitude of 3 meV/decade, which is characteristic to donor-acceptor pair recombination as well as to a semiconductor

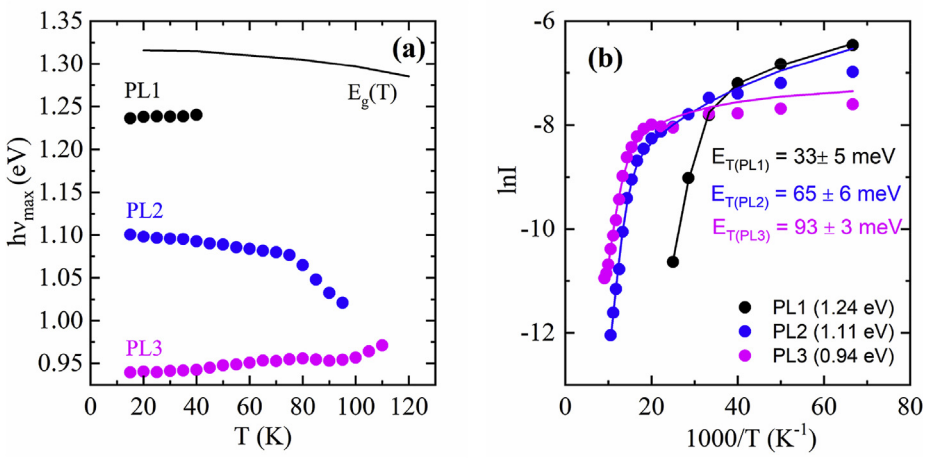

Fig. 4. The temperature dependence of the PL band peak positions together with the band gap energy E_g from Ref. [5] presented as solid line (a), and the Arrhenius plot (b) showing the thermal activation energies for the studied three PL bands in Sb_2Se_3 obtained from the fitting of the curves with Eq. (2).

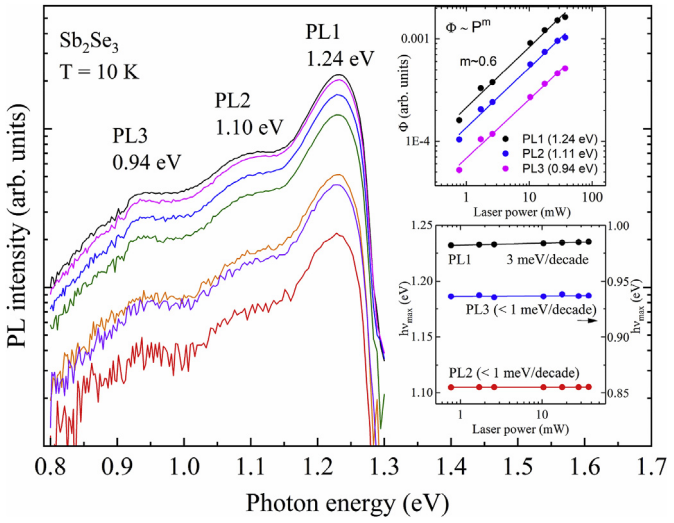

Fig. 5. The laser power dependence of the PL bands of Sb_2Se_3 at T = 10 K. The inset graphs present the laser power dependencies of the PL bands peak positions (bottom graph) and intensities (upper graph).

involving band tails [20]. The emission energy from a donor-acceptor pair separated by a distance r can be calculated by the following equation [23]:

$$h\nu_{max} = E_g - (E_a + E_d) + \frac{e^2}{4\pi\varepsilon_0\varepsilon r}, \quad (3)$$

where E_g is the bandgap energy, E_a and E_d are the acceptor and donor ionization energies, respectively, r is the distance between the donor and acceptor, e is the electron charge, ε is the static dielectric constant, and ε_0 is the permittivity of vacuum. The last term of Eq. (3) describes the Coulomb interaction between the donor and acceptor defects. The relatively small shift of the PL3 band with laser power and rather "deep" peak position indicate to the DAP recombination via very close donor-acceptor pairs, while the PL1 band involves DAP with larger distance between donor and acceptor defects.

Due to a low symmetry of Sb_2Se_3 crystal lattice, 2 different lattice sites for Sb and 3 different sites for Se exist [24]. The closest distance $r = 0.2588$ nm is between Se(1) and Sb(2) sites corresponding to the Coulomb energy of 232 meV ($\varepsilon = 24$ [11]). Considering the peak position of the PL3 band, the thermal activation energy, and the bandgap energy of Sb_2Se_3, similar value for the Coulomb energy for the PL3 band is expected. Accordingly, our results show that we have a donor-acceptor pair, where the donor and acceptor defects occupy closest Se and Sb sites in the lattice. These so-called deep donor-deep acceptor pairs (DD-DA) were discovered previously in CdTe [25], in chalcopyrites [26], and in kesterites [27]. It is known that the electron (hole) wave function in the deep donor (acceptor) level must be highly localized. Therefore, for more distant pairs, there is practically no overlapping of carriers wave functions and, consequently, no observable recombination emission. According to Ref. [8] all single defects in Sb_2Se_3 are quite deep and therefore they indeed can form DD-DA pairs. When paired, single acceptor and donor defect levels are pushed towards band edges and the thermal activation energy of these complexes will become quite small. While the PL1 band of more distant pairs shows a certain blueshift with increased excitation intensity, the PL3 band corresponding to DD-DA pairs practically does not shift. Moreover, DA pairs having somewhat larger separation and thus smaller Coulomb energy can cause the observed slightly asymmetric shape of the PL bands in addition to the broadening caused by the band tails. For example, Sb(1)-Se(3) sites are separated by the distance $r = 0.2664$ nm and the corresponding Coulomb energy is only about 7 meV smaller than for the closest distance.

The shallowest single acceptor defect in slightly Se-rich Sb_2Se_3 is $Se_{Sb(1)}$ defect having a depth of about 100 meV [8,11]. We can assume, that this defect is a component of DA pair responsible for the PL1 band. The corresponding donor defect is not clear and requires further studies.

The PL2 band behaves differently from the PL1 and PL3 bands referring to a different type of recombination. According to Fig. 4 (a), the PL2 band peak position shows a red-shift comparable or even slightly larger than the temperature dependence of the band gap energy and it is independent of the magnitude of the laser power. However, taking into account the PL2 band peak position, the low-temperature band gap of Sb_2Se_3 $E_g = 1.32$ eV [5,7] and the thermal activation energy for this PL band, it cannot be attributed to a simple band-to-acceptor recombination. Moreover, the observed peak position shift with temperature is an indication of the involvement of the band states in the recombination process for the PL2 band. Therefore, we propose that the most probable origin of the PL2 band is related to grain boundaries. There are different models about PL in the vicinity of grain boundaries, they all are

based on band bending and thus on local reduction of bandgap energy or the depth of defect levels. In this case, the recombination can occur through tunneling processes near grain boundaries, where a significant band bending is present. Similar model was proposed also for Z-bands in CdTe [28]. In our polycrystalline samples the concentration of grain boundaries is quite high and therefore the intensity of the PL2 band is also relatively high. Of course, further studies must be performed to clarify this recombination related to grain boundaries.

4. Conclusion

In conclusion, the results of a detailed photoluminescence study on Sb_2Se_3 as perspective absorber material for PV applications is presented. Radiative recombination in Sb_2Se_3 polycrystals was studied by temperature and laser power dependent photoluminescence spectroscopy that revealed the origin for the detected PL bands at 1.24 eV and 0.94 eV as donor-acceptor pair recombination. The PL1 band involves more distant donor-acceptor pairs while the PL3 band results from the deep donor − deep acceptor recombination. These results are in agreement with the theoretical defect calculations that predict high concentration of donor-acceptor pairs in this low symmetry quasi-one-dimensional Sb_2Se_3 material. Third PL band at 1.10 eV is proposed to be related to the grain boundaries, but requires further studies to clarify the recombination model behind this PL band.

Declaration of competing interest

The authors declare that they have no known competing financial interests or personal relationships that could have appeared to influence the work reported in this paper.

Acknowledgements

This work has been supported by institutional research funding IUT19-28 and personal research funding PUT1495 of the Estonian Ministry of Education and Research, and by the European Regional Development Fund, Project TK141.

References

[1] R. Venkatasubramanian, E. Siivola, T. Colpitts, B. O'Quinn, Thin-Film thermoelectric devices with high room-temperature figures of merit, Nature 413 (2001) 597−602, https://doi.org/10.1038/35098012.
[2] K. Zeng, D.-J. Xue, J. Tang, Antimony selenide thin-film solar cells, Semicond. Sci. Technol. 31 (2016), 063001, https://doi.org/10.1088/0268-1242/31/6/063001.
[3] W. Luo, A. Calas, C. Tang, F. Li, L. Zhou, L. Mai, Ultralong Sb_2Se_3 nanowire-based free-standing membrane anode for lithium/sodium ion batteries, ACS Appl. Mater. Interfaces 8 (2016) 35219−35226, https://doi.org/10.1021/acsami.6b11544.
[4] Y. Zhou, M. Leng, Z. Xia, J. Zhong, H. Song, X. Liu, B. Yang, J. Zhang, J. Chen, K. Zhou, J. Han, Y. Cheng, J. Tang, Solution-processed antimony selenide heterojunction solar cells, Adv. Energy Mater. 4 (2014), 1301846, https://doi.org/10.1002/aenm.201301846.
[5] M. Birkett, W.M. Linhart, J. Stoner, L.J. Phillips, K. Durose, J. Alaria, J.D. Major, R. Kudrawiec, T.D. Veal, Band gap temperature-dependence of close-space sublimation grown Sb_2Se_3 by photo-reflectance, Apl. Mater. 6 (2018), 084901, https://doi.org/10.1063/1.5027157.
[6] Z. Li, X. Liang, G. Li, H. Liu, H. Zhang, J. Guo, J. Chen, K. Shen, X. San, W. Yu, R.E.I. Schropp, 9.2%-efficient core-shell structured antimony selenide nanorod array solar cells, Nat. Commun. 10 (2019) 125, https://doi.org/10.1038/s41467-018-07903-6.
[7] C. Chen, W. Li, Y. Zhou, C. Chen, M. Luo, X. Liu, K. Zeng, B. Yang, C. Zhang, J. Han, J. Tang, Optical properties of amorphous and polycrystalline Sb_2Se_3 thin films prepared by thermal evaporation, Appl. Phys. Lett. 107 (2015), 043905, https://doi.org/10.1063/1.4927741.
[8] M. Huang, P. Xu, D. Han, J. Tang, S. Chen, Complicated and unconventional defect properties of the quasi-one-dimensional photovoltaic semiconductor Sb_2Se_3, ACS Appl. Mater. Interfaces 11 (2019) 15564−15572, https://doi.org/10.1021/acsami.9b01220.
[9] H. Guo, Z. Chen, X. Wang, Q. Cang, X. Jia, C. Ma, N. Yuan, J. Ding, Enhancement in the efficiency of Sb_2Se_3 thin-film solar cells by increasing carrier concentration and inducing columnar growth of the grains, Sol. RRL 3 (2019), 1800224, https://doi.org/10.1002/solr.201800224.
[10] X. Liu, X. Xiao, Y. Yang, D.J. Xue, D. Li, C. Chen, S. Lu, L. Gao, Y. He, G. Wang, S. Chen, J. Tang, Enhanced Sb_2Se_3 solar cell performance through theory-guided defect control, Prog. Photovolt. Res. Appl. 25 (2017) 861−870, https://doi.org/10.1002/pip.2900.
[11] C. Chen, D.C. Bobela, Y. Yang, S. Lu, K. Zeng, C. Ge, B. Yang, L. Gao, Y. Zhao, M.C. Beard, J. Tang, Characterization of basic physical properties of Sb_2Se_3 and its relevance for photovoltaics, Front. Optoelectron. 10 (2017) 18−30, https://doi.org/10.1007/s12200-017-0702-z.
[12] X. Wen, C. Chen, S. Lu, K. Li, R. Kondrotas, Y. Zhao, W. Chen, L. Gao, C. Wang, J. Zhang, G. Niu, J. Tang, Vapor transport deposition of antimony selenide thin film solar cells with 7.6% efficiency, Nat. Commun. 9 (2018) 2179, https://doi.org/10.1038/s41467-018-04634-6.
[13] J. Tao, X. Hu, Y. Hong, K. Li, J. Jiang, S. Chen, C. Jing, F. Yue, P. Yang, C. Zhang, Z. Wu, J. Tang, J. Chu, Investigation of electronic transport mechanisms in Sb_2Se_3 thin-film solar cells, Sol. Energy Mater. Sol. Cells 197 (2019) 1−6, https://doi.org/10.1016/j.solmat.2019.04.003.
[14] A. Shongalova, M.R. Correia, J.P. Teixeira, J.P. Leitão, J.C. González, S. Ranjbar, S. Garud, B. Vermang, J.M.V. Cunha, P.M.P. Salomé, P.A. Fernandes, Growth of Sb_2Se_3 thin films by selenization of RF sputtered binary precursors, Sol. Energy Mater. Sol. Cells 187 (2018) 219−226, https://doi.org/10.1016/j.solmat.2018.08.003.
[15] T. Raadik, J. Krustok, M.V. Yakushev, Photoreflectance study of $AgGaTe_2$ single crystals, Phys. B Condens. Matter 406 (2011) 418−420, https://doi.org/10.1016/j.physb.2010.11.002.
[16] L.J. Phillips, C.N. Savory, O.S. Hutter, P.J. Yates, H. Shiel, S. Mariotti, L. Bowen, M. Birkett, K. Durose, D.O. Scanlon, J.D. Major, Current enhancement via a TiO_2 window layer for CSS Sb_2Se_3 solar cells: performance limits and high voc, IEEE J. Photovolt. 9 (2019) 544−551, https://doi.org/10.1109/JPHOTOV.2018.2885836.
[17] A. Shongalova, M.R. Correia, B. Vermang, J.M.V. Cunha, P.M.P. Salome, P.A. Fernandes, On the identification of Sb_2Se_3 using Raman scattering, MRS Commun. 8 (2018) 865−870, https://doi.org/10.1557/mrc.2018.94.
[18] D.E. Aspnes, Handbook on Semiconductors. Vol. 2. Optical Properties of Solids, North- Holland Publishing Company, Amsterdam, 1980.
[19] J. Krustok, H. Collan, M. Yakushev, K. Hjelt, The role of spatial potential fluctuations in the shape of the PL bands of multinary semiconductor compounds, Phys. Scr. T79 (1999) 179−182, https://doi.org/10.1238/Physica.Topical.079a00179.
[20] A.P. Levanyuk, V.V. Osipov, Edge luminescence of direct-gap semiconductors, Sov. Phys. Uspekhi 24 (1981) 187−215, https://doi.org/10.1070/PU1981v024n03ABEH004770.
[21] J. Krustok, H. Collan, K. Hjelt, Does the low-temperature Arrhenius plot of the photoluminescence intensity in CdTe point towards an erroneous activation energy? J. Appl. Phys. 81 (1997) 1442, https://doi.org/10.1063/1.363903.
[22] T. Schmidt, K. Lischka, W. Zulehner, Excitation-power dependence of the near-band-edge photoluminescence of semiconductors, Phys. Rev. B 45 (1992) 8989, https://doi.org/10.1103/PhysRevB.45.8989.
[23] F. Williams, Donor—acceptor pairs in semiconductors, Phys. Status Solidi 25 (1968) 493−512, https://doi.org/10.1002/pssb.19680250202.
[24] V.L. Deringer, R.P. Stoffel, M. Wuttig, R. Dronskowski, Vibrational properties and bonding nature of Sb_2Se_3 and their implications for chalcogenide materials, Chem. Sci. 6 (2015) 5255−5262, https://doi.org/10.1039/c5sc00825e.
[25] J. Krustok, H. Collan, K. Hjelt, J. Mädasson, V. Valdna, Photoluminescence from deep acceptor-deep donor complexes in CdTe, J. Lumin. 72−74 (1997) 103−105, https://doi.org/10.1016/S0022-2313(97)00061-6.
[26] J. Krustok, J. Raudoja, J.H. Schön, M. Yakushev, H. Collan, The role of deep donor- deep acceptor complexes in CIS- related compounds, Thin Solid Films 361−362 (2000) 406−410, https://doi.org/10.1016/S0040-6090(99)00756-7.
[27] J. Krustok, T. Raadik, M. Grossberg, M. Kauk-Kuusik, V. Trifiletti, S. Binetti, Photoluminescence study of deep donor- deep acceptor pairs in Cu_2ZnSnS_4, Mater. Sci. Semicond. Process. 80 (2018) 52−55, https://doi.org/10.1016/j.mssp.2018.02.025.
[28] J. Krustok, J. Mädasson, J. Hiie, Photoluminescence properties of Z- bands in CdTe, Phys. Status Solidi (a) 165 (1998) 517−525, https://doi.org/10.1002/(SICI)1521-396X(199802)165:2%3C517::AID-PSSA517%3E3.0.CO;2-O.